SEARCH FOR CRITICAL BEHAVIOUR OF STRONGLY INTERACTING MATTER AT THE CERN SUPER PROTON SYNCHROTRON

M. Gazdzicki[a,b], P. Seyboth[c,b]

[a]Goethe-University, Frankfurt, Germany
[b]Jan Kochanowski University, Kielce, Poland
[c]Max-Planck-Institut für Physik, Munich, Germany

(Received March 4, 2016)

History, status and plans of the search for critical behaviour of strongly interacting matter created in nucleus–nucleus collisions at the CERN Super Proton Synchrotron is reviewed. In particular, it is expected that the search should answer the question whether the critical point of strongly interacting matter exists and, if it does, where it is located. First, the search strategies are presented and a short introduction is given to expected fluctuation signals and to the quantities used by experiments to detect them. The most important background effects are also discussed. Second, relevant experimental results are summarized and discussed. It is intriguing that both the fluctuations of quantities integrated over the full experimental acceptance (event multiplicity and transverse momentum) as well as the bin size dependence of the second factorial moment of pion and proton multiplicities in medium-sized Si+Si collisions at 158A GeV/c suggest critical behaviour of the created matter. These results provide strong motivation for the ongoing systematic scan of the phase diagram by the NA61/SHINE experiment at the SPS and the continuing search at the Brookhaven Relativistic Hadron Collider.

DOI:10.5506/APhysPolB.47.1201

1. Introduction

The structure of the phase diagram of strongly interacting matter is one of the most important topics in nuclear and particle physics. We know that at low densities, strongly interacting particles are hadrons and thus the matter is in form of a hadron gas or liquid. Since the discovery of sub-hadronic particles, quarks and gluons, it was speculated that at high temperature and/or pressure, densely packed hadrons will "dissolve" into a new phase of quasi-free quarks and gluons, the quark–gluon plasma (QGP) [1].

Many years of intense experimental and theoretical studies of high energy nucleus–nucleus ($A+A$) collisions led to the conclusion that the quark–gluon plasma exists in nature. This conclusion is based on a wealth of systematic data on $A+A$ collisions at very high energies from the CERN Large Hadron Collider (LHC) [2] and the BNL Relativistic Heavy Ion Collider (RHIC) (see *e.g.* Ref. [3]), and, very importantly, the observation of the transition between hadronic matter and quark–gluon plasma at the CERN Super Proton Synchrotron energies [4] (for recent review, see Refs. [5, 6]).

Thus, the current key question in the study of the phase diagram of strongly interacting matter is the structure of the phase transition region between the hadron gas and the quark–gluon plasma.

The most popular suggestion is shown schematically in Fig. 1. The transition at low temperature T and high baryochemical potential μ_B is believed to be of the first order and happen along a line which ends with decreasing μ_B in a critical point (of the second order) and then, turns into a crossover region. The non-trivial structure of the phase transition region was first suggested by Asakawa, Yazaki [7] and Barducci, Casalbuoni, De Curtis, Gatto, Pettini [8]. Experimental studies of the features of the phase diagram were strongly motivated by predictions of measurable effects. The pioneering work of Wosiek [9] pointed out that intermittent [10] behaviour is naturally expected at a phase transition of the second order. Soon after that, the conjecture was further developed by Satz [11], Antoniu *et al.* [12] and Bialas, Hwa [13]. This initiated experimental studies of the structure of the phase transition region via studies of particle multiplicity fluctuations using scaled factorial moments. Later, additional measures of fluctuations

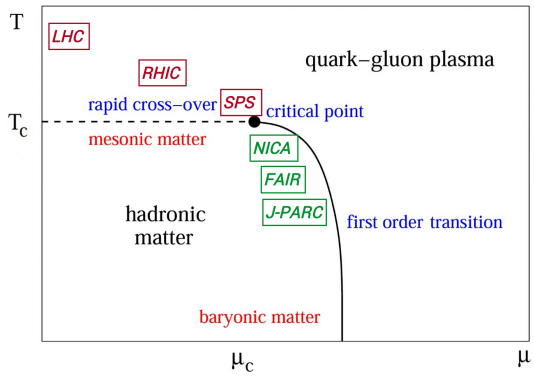

Fig. 1. (Colour on-line) Sketch of the phase diagram of strongly interacting matter. Italic labels added to the sketch show regions probed by the early stage of heavy ion collisions studied in current (in black/red) and future (in light grey/green) experimental programmes.

were also proposed as probes of critical behaviour [14, 15]. The results of the KLM [16] and NA49 [17] experiments suggest that effects related to the critical point may have been observed in collisions of medium size nuclei at the top SPS energy. This motivated the NA61/SHINE experiment to perform a systematic scan in collision energy and system size. The new measurements should answer the general question about the nature of the transition region and, in particular, the question: *does the critical point of strongly interacting matter exist in nature and, if it does, where is it located?* The most recent experimental and theoretical status of the exploration of the phase diagram is reviewed at the regular workshops on the Critical Point and Onset of Deconfinement [18].

The structure of the transition region is explored experimentally by studying the final states produced in nucleus–nucleus collisions. By changing collision energy and size of colliding nuclei, one changes temperature T and chemical potential μ_B of matter at the freeze-out stage [19]. In particular, by increasing collision energy more and more pions per colliding baryon are produced, which is the main cause for the decrease of the baryon chemical potential with collision energy. With increasing size of the colliding nuclei, the volume of created matter increases and, consequently, the role of hadron–hadron interactions at the late stage of matter evolution becomes more important. This leads to a decrease of the freeze-out temperature with increasing size of the colliding nuclei. Thus, scanning in collision energy and system size, one hopes to be able to move the freeze-out close to the transition region. This is illustrated in Fig. 2. The left plot shows the collision energy dependence of the freeze-out parameters in central Pb+Pb collisions [20–23], whereas the right one presents their energy and system size dependence at the CERN SPS [19].

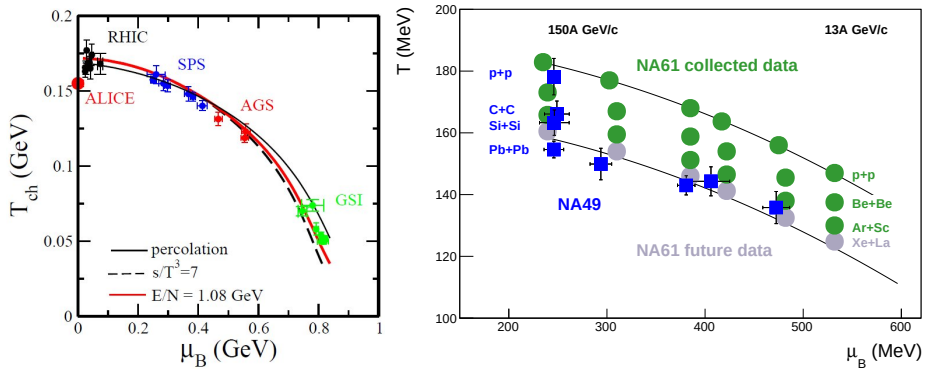

Fig. 2. Left: Compilation of chemical freeze-out points of central Pb+Pb (Au+Au) collisions [20]. Right: Chemical freeze-out points of nucleus–nucleus collisions studied with the NA49 [19] and NA61/SHINE [31] programmes at the CERN SPS.

The experimental search for the critical point by investigating nuclear collisions is promising only at energies higher than the energy of the onset of deconfinement, which experimentally was located to be at the low SPS energies [24, 25]. This is because the energy density at the early stage of the collision, which is required for the onset of deconfinement is higher than the energy density at freeze-out, which is relevant for the search for the critical point.

A characteristic feature of a second-order phase transition (the critical point or line) is the divergence of the correlation length. The system becomes scale invariant. This leads to large fluctuations in particle multiplicity. Moreover, these fluctuations have specific characteristics [9, 13]. Also other properties of the system should be sensitive to the vicinity of the critical point [15]. Thus, when scanning the phase diagram, a region of increased fluctuations may signal the critical point or the critical line. This is illustrated schematically in Fig. 3 which presents an updated version of the plot shown first in Ref. [26].

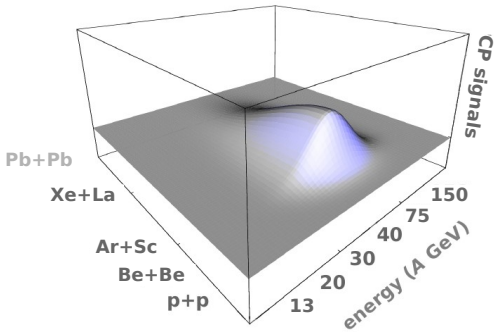

Fig. 3. Sketch of the "critical hill" expected in the search for the critical point in the two-dimensional plane (system size)–(collision energy). At the hill, the characteristic fluctuation signals of the critical point are maximal, see Sec. 2.5 for details.

The study of fluctuations and correlations is significantly more difficult than the study of single particle spectra and mean multiplicities. In general, results on fluctuations are sensitive to conservation laws, resonance decays and many of them also to the unavoidable volume fluctuations of colliding nuclear matter. Moreover, they cannot be corrected for a limited experimental acceptance.

This review is organized as follows. In Sec. 2, experimental strategies, as well as techniques and problems for the search for the critical point are briefly presented. Search results from experiments at the CERN SPS, in particular NA49 and NA61/SHINE, are reviewed in Sec. 3. Conclusions and an outlook in Sec. 4 close the paper.

2. Search strategies, techniques and problems

This section reviews basic ideas and tools relevant for the experimental search for the critical behaviour of strongly interacting matter at the CERN SPS. The most important background effects are listed and examples are discussed.

2.1. Onset of deconfinement versus critical point

Here, relations between the onset of deconfinement, the critical point of strongly interacting matter and the possibilities of their experimental study in relativistic nucleus–nucleus collisions are discussed. The two sketches presented in Fig. 4 should help to understand the basic ideas.

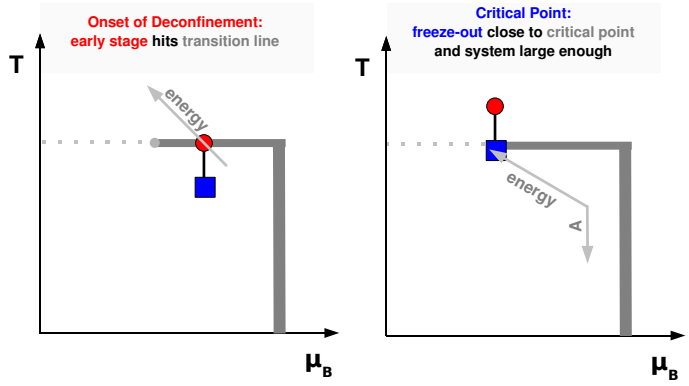

Fig. 4. Sketch of the search strategy for the onset of deconfinement (left) and the critical point (right). The location in the phase diagram of the matter at the early stage is indicated by the black/red dot and at freeze-out by the black/blue square. The solid (dotted) lines show the first order- (rapid crossover) boundary and the critical point is the light grey dot at the end of the first-order transition line.

The onset of deconfinement refers to the beginning of the creation of a deconfined state of strongly interacting matter (ultimately a quark–gluon plasma) at the early stage of nucleus–nucleus collisions when increasing the collision energy. With increasing collision energy, the energy density of matter created at the early stage of $A + A$ collisions increases[1]. Thus, if there are two phases[2] of matter separated by the transition region (solid and

[1] The correlation between collision energy and the early stage energy density is expected to be strong for central collisions of large nuclei and weak for collisions of low mass nuclei. In the latter case, energy and/or multiplicity of produced particles may help select collisions with a similar energy density.

[2] The discussed two-phase diagram is the simplest one which allows to introduce the concepts of the onset of deconfinement and the transition region. There are numerous suggestions of phase diagrams with a much richer structure (see *e.g.*, Ref. [30]).

dotted lines) as indicated in Fig. 4 (left), the early stage (the black/red point) has to cross the transition region. Therefore, the existence of the onset of deconfinement is the most straightforward consequence of the existence of two phases of strongly interacting matter, *i.e.* confined matter and QGP. The experimental observation of the onset of deconfinement required a one-dimensional scan in collision energy with heavy ions as performed by NA49 [24]. Signals of the onset of deconfinement relate to the difference in properties of confined matter and QGP. They are weakly sensitive to the structure of the transition region.

Discovery of the onset of deconfinement implies the existence of QGP and of a transition region between confined and QGP phases. Recent experimental results [25] indicate that the transition region (the mixed phase or rapid cross-over) ranges from $\sqrt{s_{NN}} \approx 8$ GeV to $\sqrt{s_{NN}} \approx 12$ GeV, where $\sqrt{s_{NN}}$ denotes collision energy per nucleon pair in the centre-of-mass system.

Numerous possibilities concerning the structure of the transition region are under discussion (see *e.g.*, Ref. [27]). The most popular one [28, 29], sketched in Fig. 4, claims that a 1$^{\text{st}}$ order phase transition (thick grey line) separates both phases in the high baryonic chemical potential domain. In the low baryonic chemical potential domain, a rapid crossover is expected (dotted line). The end point of the 1$^{\text{st}}$ order phase transition line (light grey dot in Fig. 4) is the critical point (of the second order).

The characteristic signatures of the critical point can be observed if the freeze-out point (black/blue square in Fig. 4 (right)) is located close to the critical point. The analysis of the existing experimental data [19] indicates that the location of the freeze-out point in the phase diagram depends on the collision energy and the mass of the colliding nuclei. This dependence is schematically indicated in Fig. 4 (right) and quantified in Fig. 2 (right). Thus, the experimental search for the critical point requires a two-dimensional scan in collision energy and size of the colliding nuclei. The NA61/SHINE experiment [26, 31] at the CERN SPS started this scan in 2009 and completion is expected within the coming few years. Note, that a two-dimensional scan is actually required for any study of the structure of the transition region, independent of the hypothesis tested.

The transition region can be studied experimentally in nucleus–nucleus collisions only at T, μ_{B} values which correspond to collision energies higher than the energy of the onset of deconfinement. This important conclusion is easy to understand when looking at Fig. 4. Signals of the transition region can be observed provided the freeze-out point is close to it (see Fig. 4 (right)). Furthermore, the energy density at the early stage of the collision is, of course, higher than the energy density at freeze-out. Thus, the condition that the freeze-out point is near the transition region implies that the early stage of the system is above (or on) it. This, in turn, means that the

optimal energy range for the search for the critical point (or, in general, for the study of properties of the transition region) lies above the energy of the onset of deconfinement (see Fig. 4 (left)). This general condition limits the search for the critical point to the collision energy range $E_{\mathrm{LAB}} > 30A$ GeV ($\sqrt{s_{NN}} \approx 8$ GeV).

2.2. Scaled factorial moments

In the grand canonical ensemble, the correlation length ξ diverges at the critical point (or second-order phase transition line) and the system becomes scale invariant [9, 11]. This leads to large multiplicity fluctuations with special properties. They can be conveniently exposed using scaled factorial moments $F_r(\delta)$ [10] of rank (order) r

$$F_r(\delta) = \frac{\left\langle \frac{1}{M}\sum_{i=1}^{M} N_i(N_i-1)\dots(N_i-r+1)\right\rangle}{\left\langle \frac{1}{M}\sum_{i=1}^{M} N_i\right\rangle^r}\,, \tag{1}$$

where δ is the size of the subdivision intervals of the momentum phase-space region Δ and $M = \Delta/\delta$ is the number of intervals. N_i refers to particle multiplicity in the interval i and $\langle \dots \rangle$ indicates averaging over the analysed collisions.

For a non-interacting (ideal) gas of Boltzmann particles in the grand canonical ensemble (IB-GCE), one gets $F_r(\delta) = 1$ for all values of r and δ provided the mean particle multiplicity is proportional to δ. The latter condition is trivially obeyed for a subdivision in configuration space where the particle density is uniform throughout the gas volume. For the case of subdivision in momentum space, the subdivision should be performed using so-called cumulative kinematic variables [32] in which the particle density is uniform.

At the second-order phase transition, the matter properties strongly deviate from the ideal gas. The system is a simple fractal and $F_r(\delta)$ possess a power law dependence on δ

$$F_r(\delta) = F_r(\Delta)\,(\Delta/\delta)^{\phi_r}\,. \tag{2}$$

Moreover, the exponent (intermittency index) ϕ_r satisfies the relation

$$\phi_r = (r-1)\,d_r\,, \tag{3}$$

with the anomalous fractal dimension d_r being independent of r [13]. These results are valid when cumulative variables [32] are used to define the intervals δ. The properties represented by Eqs. (2) and (3) are called in this paper the critical behaviour of the scaled factorial moments.

An experimental search for the properties (2) and (3) in high energy collisions requires significant additional input. In particular, one has to decide on:

(i) dimension, size and location of the momentum phase-space region Δ,

(ii) selection of collisions used in the analysis,

(iii) selection of particles used in the analysis.

Concerning *(i)*, it was shown by Bialas, Seixas [33] (see also Ochs, Wosiek [34, 35]) that unbiased results on the critical behaviour of scaled factorial moments can be obtained only by performing the analysis in variables and dimensions in which the singular behaviour appears. Any projection procedure is likely to remove, at least partly, the critical fluctuation signal.

Concerning *(iii)*, QCD-inspired considerations [28, 36] suggest that the order parameter of the phase transition is the chiral condensate $\langle \bar{q}q \rangle$ (q is the quark field). The quantum state carrying the quantum numbers as well as the critical properties of the chiral condensate is the isoscalar σ field. Assuming that this state can be formed in high energy collisions, there are two possibilities for the observation of the properties (2) and (3):

(i) Directly from its decay products [37]. The condensate will decay into $\pi^+\pi^-$ pairs with invariant mass just above twice the pion mass. Detection of the expected fluctuations requires reconstruction of the pion pairs. One expects here $d = \phi_2 = 2/3$ [37].

(ii) Through measuring the fluctuations of the proton number. The net-baryon density mixes with the chiral condensate transferring the critical fluctuations to the net-baryon density [28, 38–43], which is an equivalent order parameter of the phase transition. The resulting fluctuations are predicted to be present also in the net-proton number as well as in the proton and anti-proton numbers separately [44]. One expects here $d = \phi_2 = 5/6$ [45].

2.3. Central moments

The infinite correlation length at a second-order phase transition is expected to lead to divergence of the second central moment of the multiplicity distribution. This was recently illustrated by Vovchenko, Anchinshkin, Gorenstein and Poberezhnyuk [46, 47] via analytical calculations performed in the GCE for a gas obeying the van der Waals equation of state. As seen in Fig. 5, the scaled variance $\omega = (\langle N^2 \rangle - \langle N \rangle^2)/\langle N \rangle$ increases when the critical point is approached and it diverges at the critical point.

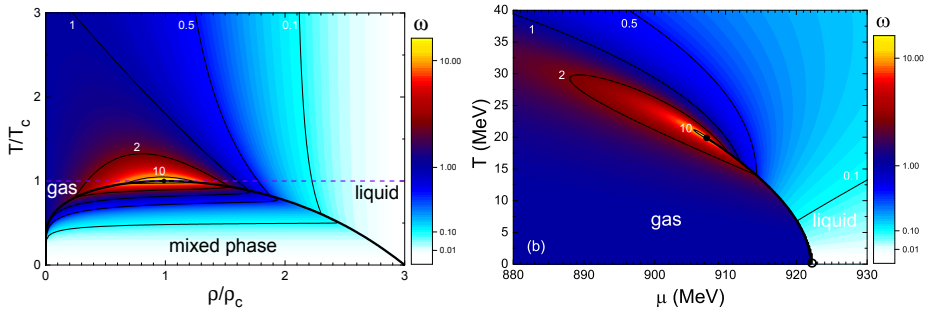

Fig. 5. Left: Scaled variance of the multiplicity distribution calculated within the grand canonical formulation of the van der Waals model (massless particles obeying Boltzmann statistics) as a function of temperature T and particle density ρ scaled by the corresponding values at the critical point (from Ref. [46]). Right: Scaled variance of the multiplicity distribution calculated within the grand canonical formulation of the van der Waals model (nucleons obeying Fermi statistics) as a function of temperature T and baryon chemical potential μ (from Ref. [47]).

Moments of other quantities are also expected to increase in the vicinity of the critical point. In particular, these are event transverse momentum (vector magnitudes are summed) and net charges of produced particles [15]. Of course, the latter have to be studied in a phase-space region which covers only a small fraction of all particles in order to avoid suppression of fluctuations due to conservation laws (see below for details).

It was pointed out by Stephanov [48] that second moments of the multiplicity distribution increase in proportion to the square of the correlation length, while moments of higher order are proportional to even higher powers of the correlation length. Moreover, ratios of certain higher order cumulants are expected to be independent of the correlation length and, therefore, allow a consistency test [49]. Based on QCD model calculations, the same paper also presents quantitative estimates of the size of the enhancement of multiplicity fluctuations caused by a critical point.

2.4. Strongly intensive quantities

Since event-to-event volume fluctuations cannot be eliminated in experimental studies of nucleus–nucleus collisions, it is important to minimise their effect by defining suitable fluctuation measures. It appears that using second and first moments of the distribution of two extensive quantities (their first moments are proportional to volume), one can construct fluctuation measures which are, within a statistical model of the ideal Boltzmann gas in the grand canonical ensemble formulation (SM(IB-GCE)) [50], independent of its fluctuations.

As the simplest example, let us consider multiplicities of two different types of hadrons, A and B. Their mean multiplicities are proportional to the system volume

$$\langle A\rangle \sim V\,, \qquad \langle B\rangle \sim V\,. \tag{4}$$

Obviously, the ratio of mean multiplicities is independent of the volume V. Moreover, the ratio $\langle A\rangle/\langle B\rangle$ is independent of $P(V)$, where $P(V)$ is the probability (density) distribution of V for the considered set of collisions. Quantities which have the latter property are called strongly intensive quantities [50]. Such quantities are recommended to be used in experimental studies of the system size dependence of fluctuations in $A+A$ collisions as they eliminate the influence of usually poorly known distributions of the system volume.

More generally, A and B can be any extensive event quantities such as the sum of transverse momenta, the net charge or the multiplicity of a particular type of particle. The scaled variances of A and B and the mixed second moment $\langle AB\rangle$ calculated within the SM(IB-GCE) [50] read:

$$\omega[A] = \omega^*[A] + \langle A\rangle/\langle V\rangle\,\omega[V]\,, \tag{5}$$

$$\omega[B] = \omega^*[B] + \langle B\rangle/\langle V\rangle\,\omega[V]\,, \tag{6}$$

$$\langle AB\rangle = \langle AB\rangle^*\langle V\rangle + \langle A\rangle\langle B\rangle\langle V\rangle^2\,\left(\langle V^2\rangle - \langle V\rangle\right)\,, \tag{7}$$

where quantities denoted by * are quantities calculated for a fixed value of the system volume.

From Eqs. (5)–(7) follows [50, 51] that suitably constructed functions of the second moments, namely

$$\Delta[A,B] = \frac{1}{C_\Delta}\left[\langle B\rangle\,\omega[A] - \langle A\rangle\,\omega[B]\right] \tag{8}$$

and

$$\Sigma[A,B] = \frac{1}{C_\Sigma}\left[\langle B\rangle\,\omega[A] + \langle A\rangle\,\omega[B] - 2\left(\langle AB\rangle - \langle A\rangle\langle B\rangle\right)\right] \tag{9}$$

are independent of $P(V)$ in the SM(IB-GCE). Here, the normalisation factors C_Δ and C_Σ are required to be proportional to first moments of any extensive quantities. In Ref. [51], a specific choice of the C_Δ and C_Σ normalisation factors was proposed which makes the quantities $\Delta[A,B]$ and $\Sigma[A,B]$ dimensionless and leads to $\Delta[A,B] = \Sigma[A,B] = 1$ in the independent particle model (IPM). This normalisation is called here the IPM normalisation and unless otherwise stated, the IPM normalisation is used.

Thus, $\Delta[A,B]$ and $\Sigma[A,B]$ are strongly intensive quantities which measure fluctuations of A and B, *i.e.* they are sensitive to second moments of the distributions of the quantities A and B. Results on $\Delta[A,B]$ and $\Sigma[A,B]$ are referred to as results on A–B fluctuations, *e.g.* transverse momentum–multiplicity fluctuations.

For the case of multiplicity A–multiplicity B fluctuations, the expressions for $\Delta[A,B]$ and $\Sigma[A,B]$ with the IPM normalisation read

$$\Delta[A,B] = (\langle B\rangle\omega[A] - \langle A\rangle\omega[B])/(\langle B\rangle - \langle A\rangle) \tag{10}$$

and

$$\Sigma[A,B] = (\langle B\rangle\omega[A] + \langle A\rangle\omega[B] - 2(\langle AB\rangle - \langle A\rangle\langle B\rangle))/(\langle B\rangle + \langle A\rangle)\,. \tag{11}$$

The Σ quantity is a reincarnation of the popular Φ measure of fluctuations [52]. The original definition of Φ is

$$\Phi_x = \sqrt{\frac{\langle Z^2\rangle}{\langle N\rangle}} - \sqrt{\overline{(x-\overline{x})^2}}\,, \tag{12}$$

where x and $\overline{x}$ are a single particle quantity and its mean value, respectively, and

$$Z = \sum_{i=1}^{N}(x_i - \overline{x}) \tag{13}$$

with the sum running over the N particles in the event. Φ was shown to be related to Σ as follows [50]:

$$\Phi_x = \sqrt{\overline{x}\omega[x]}\left[\sqrt{\Sigma[X,N]} - 1\right] \tag{14}$$

with $X = \sum_{i=1}^{N} x_i$ and $C_\Sigma = \langle N\rangle\omega[x]$.

By construction, strongly intensive measures of fluctuations are always a functional of two extensive quantities. This, in general, hampers a straightforward interpretation of experimental results. However, under certain conditions, the Δ quantity can be used to obtain the scaled variance of the extensive quantity A separately.

Let A be the extensive quantity, *e.g.* selected for its sensitivity to the critical fluctuations. Then, choose a quantity B which is proportional to the system volume $B \sim V$. Then, it is easy to show that the strongly intensive measures $\Delta_B[A,B]$ and $\Sigma_B[A,B]$ (equal to $\Delta[A,B]$ and $\Sigma_B[A,B]$ with the normalisation $C_\Delta = \langle B\rangle \sim V$) obey the relation

$$\Delta_B[A,B] = \Sigma_B[A,B] = \omega^*[A]\,. \tag{15}$$

In the derivation of Eq. (15), one assumes the validity of Eq. (5) which needs to be investigated case-by-case. Thus, $\Delta_B[A,B]$ is approximately equal to the scaled variance $\omega^*[A]$ of A for a fixed system volume (see Eq. (5))

$$\Delta_B[A,B_V] \approx \omega^*[A]\,. \tag{16}$$

Suggestions of practical choices of A and B are:

(i) A — multiplicity of hadrons which are sensitive to the critical behaviour, *e.g.* protons, sigma-mesons, pions in the central rapidity window and

(ii) B — net electric charge in full phase space or large acceptance excluding fragmentation regions of projectile and target nuclei; it is equal to the number of participant protons and thus approximately proportional to the volume of matter involved in the collision or
— the number of projectile participants calculated as the difference between the number of nucleons in the beam nuclei and the number of projectile spectators measured by a "zero degree" calorimeter, *e.g.*, the Projectile Spectator Detector of NA61/SHINE.

Recently, strongly intensive measures which involve higher than second moments were proposed [53]. The next important step would be to reformulate the critical properties of scaled factorial moments Eqs. (2) and (3) in terms of strongly intensive quantities.

2.5. Critical hill

As discussed in Sec. 2.3, moments of multiplicity distribution diverge when temperature and density approach their critical values (see Fig. 5). At this same point in the phase diagram, the scaled factorial moments should obey the critical properties described by Eqs. (2) and (3).

As previously argued, the freeze-out temperature increases with increasing collision energy and decreasing size of the colliding nuclei. The maximum temperature, probably the closest to the phase transition, is observed in $p+p$ interactions. However, the small volume and short life-time of the created matter together with the conservation laws (see the next section), do not allow the divergence of the correlation length [49, 54]. Thus, neither a divergence of fluctuation measures, *e.g.* of the scaled variance, nor the appearance of critical behaviour of scaled factorial moments are expected.

On the other hand, critical fluctuations developing in the system produced by collisions of large nuclei may be erased by re-scattering processes between hadronisation and kinetic freeze-out. Therefore, one can argue that the maximal signals of the critical point may be observed for collisions of

medium mass nuclei. In this case, the volume and life-time of the created matter are large enough to allow for the critical behaviour to appear, and the temperature is close enough to the critical temperature to make the critical behaviour visible. Thus observation of the "critical hill", as sketched in Fig. 3, would provide convincing evidence for the existence and location of the critical point.

2.6. Background fluctuations

The critical hill, if observed, will rise above a background caused by many different sources of fluctuations. These are, in particular,

(i) volume fluctuations discussed in Sec. 2.4,

(ii) conservation laws discussed in Sec. 2.7,

(iii) formation and decay of resonances,

(iv) quantum statistical effects (Bose–Einstein and Fermi–Dirac statistics).

Their impact on fluctuations is discussed in the recent review [55] where also references to original papers are given.

In general, the background fluctuations are not expected to lead to non-monotonic dependence of fluctuations on collision energy and system size.

The effect of volume fluctuations is addressed in Sec. 2.4. As an additional example, the effect of conservation laws is discussed below, in more detail.

2.7. Conservation laws

Predictions of statistical models concerning the volume dependence change qualitatively when material and/or motional conservation laws are introduced, *i.e.* instead of the grand canonical ensemble, the canonical (CE) or micro-canonical (MCE) ensembles are used. The effect of conservation laws has been extensively studied for mean multiplicities since 1980 (see, *e.g.* Refs. [56–58]) and for second moments of multiplicity distributions since 2004 (see, *e.g.* Refs. [59, 60]). An example is discussed below for illustration.

Figure 6, taken from Ref. [59], presents the results of calculations performed within the simplest model which allows to study the effect of material conservation laws on mean multiplicity and scaled variance of the multiplicity distribution. In this model, an ideal gas of classical positively and negatively charged particles is assumed. The ratio of the mean multiplicities calculated within the SM(IB-CE) and the SM(IB-GCE) is plotted in Fig. 6 (left) as a function of the mean multiplicity z from the SM(IB-GCE), the latter being proportional to the system volume. The ratio approaches one with

increasing volume. Thus, for sufficiently large systems, mean multiplicities obtained within the SM(IB-GCE) can be used instead of mean multiplicities from the SM(IB-CE) and the SM(IB-MCE) [60]. This is, however, not the case for the scaled variance as illustrated in Fig. 6 (right). The results for the SM(IB-CE) and the SM(IB-GCE) approach each other when the volume decreases to zero. Of course, the scaled variance in the SM(IB-GCE) is the one independent of volume. Different behaviour is observed for the scaled variance in the SM(IB-CE), where it decreases with increasing volume and for a sufficiently large volume approaches 0.5.

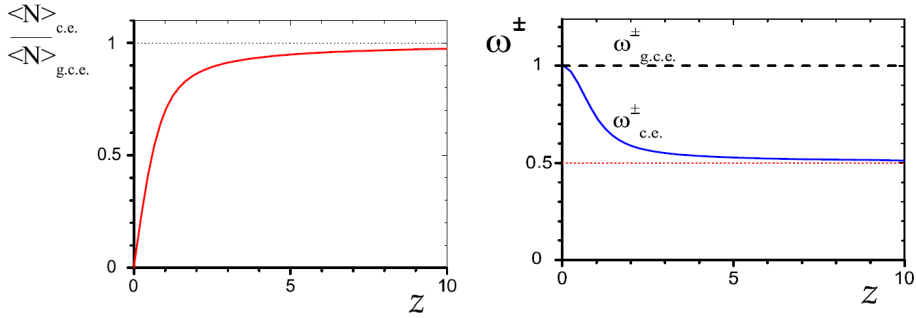

Fig. 6. The ratio of mean multiplicities $\langle N \rangle = \langle N_+ \rangle$ or $\langle N_- \rangle$ calculated within the SM(IB-CE) and the SM(IB-GCE) are plotted in the left panel as a function of mean multiplicity z for the SM(IB-GCE), with z being proportional to the system volume. The corresponding scaled variances ω^+, ω^- are shown in the right panel. The ideal gas model of classical positively and negatively charged particles was used for calculations. The system net charge is assumed to be zero and thus $\langle N_+ \rangle = \langle N_- \rangle$ and $\langle \omega^+ \rangle = \langle \omega^- \rangle$. The plots are taken from Ref. [59].

The above example clearly illustrates the importance of material and motional conservation laws for hadron production in nucleus–nucleus collisions at high energies. In particular, the conservation laws may strongly affect fluctuations even for large systems, leading to significant deviations from the simplest reference model, *i.e.* independent particle production.

3. Search results from experiments at the CERN SPS

This section reviews the status of the experimental search for evidence of a second-order phase transition and/or the critical point at the CERN SPS based on published results and preliminary data presented at conferences.

3.1. Pioneering analyses

The search for the critical behaviour of strongly interacting matter at the CERN SPS started in 1990 from the pioneering paper of Bialas and Hwa [13]. In this work, the authors compiled results from intermittency analyses performed by the EMC [61], NA22 [62] and KLM [16] experiments at the SPS. In these experiments, intermittency indices ϕ_r were determined from power-law fits to the dependence on bin-size in (pseudo-)rapidity of the scaled factorial moments of successive rank r. Figure 7 shows that the anomalous dimensions, defined as $d_r = \phi_r/(r-1)$, increase strongly with rank r for the smaller reaction systems. Interestingly, the anomalous dimension stays constant for the heaviest system, for S+(AgBr) collisions at 200A GeV/c. Bialas and Hwa interpreted this behaviour as an indication of a second-order phase transition. A quantitative prediction of d_r was not provided.

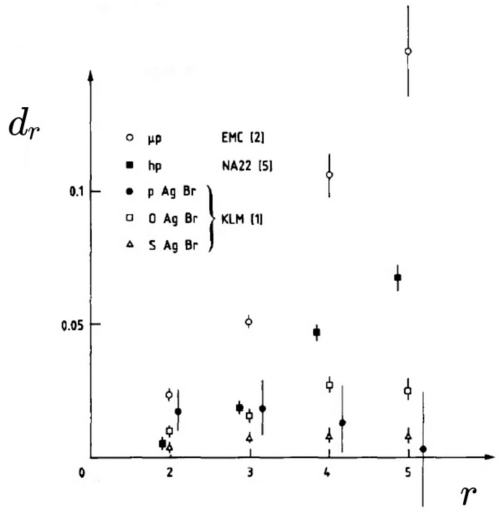

Fig. 7. Anomalous dimensions $d_r = \phi_r/(r-1)$ of pseudo-rapidity spectra of hadrons produced in $\mu + p$, $h + p$, p+AgBr, O+AgBr and S+AgBr collisions at $\sqrt{s_{NN}} \approx$ 20 GeV [13].

An extended analysis of the emulsion data of the KLM Collaboration was published in Ref. [63]. Corrections were applied for the non-uniform rapidity distribution and the intermittency indices were determined both for 1-dimensional (pseudo-rapidity) and 2-dimensional (pseudo-rapidity and azimuthal angle) subdivisions of phase space. The resulting anomalous dimensions for S+(AgBr) collisions at 200A GeV/c are plotted in Fig. 8. One observes that the values of d_r are consistent with being independent of r for both analyses and confirm the earlier results. However, the values of d_r are

roughly 5 times larger in the 2-dimensional analysis. A strong reduction of the measured power ϕ_r with decreasing dimensionality of the analysis was explained by Bialas and Seixas [33] as due to averaging of fluctuations via the projection procedure. Thus, the factorial moment analysis in three dimensions seems to be mandatory in future searches for the critical behaviour.

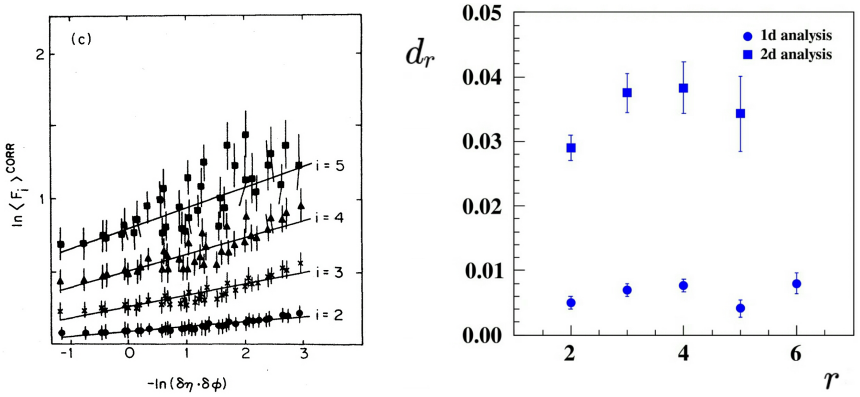

Fig. 8. Left: Scaled factorial moments of rank i from two-dimensional analysis in pseudo-rapidity and azimuthal angle as a function of subdivision size for the 19% most central S+(AgBr) collisions at 200A GeV/c [63]. Right: The corresponding anomalous dimensions d_r *versus* order r are shown by squares, whereas the circles show results for the one-dimensional analysis in pseudo-rapidity.

Motivated by these results, the WA80 [64] and NA35 [65] experiments at the SPS revisited intermittency analysis in nucleus–nucleus collisions at 200A GeV/c. WA80 did not have momentum measurement and inferior 2-track and angular resolution compared to the emulsion experiment. They concluded that they observed no significant intermittency effect in S+S and S+Au collisions when taking into account statistical and systematic uncertainties.

The NA35 streamer chamber experiment performed momentum measurements in central p+Au, O+Au, S+S and S+Au collisions which were subjected to a fully differential 3-dimensional (rapidity, transverse momentum, azimuthal angle) intermittency analysis. Although the factorial moments were found to increase with the number of subdivisions of phase space, this rise was not well-described by a power law. Instead, a conventional model supplemented by Bose–Einstein correlations provided a satisfactory description.

In summary, the intermittency analyses of charged particle production in oxygen and sulphur induced reactions did not lead to conclusive results on the existence of a second-order phase transition in these reactions. More recent theoretical investigations suggest that when the hadronization of a QGP occurs near the critical point, the hadronization of the chiral condensate will lead to intermittency in the production of protons and low-mass $\pi^+\pi^-$ pairs with known intermittency index. A search for such effects is in progress in the NA49 experiment and will be discussed below.

3.2. Systematic fluctuation studies of NA49 and NA61/SHINE

Search for evidence of critical behaviour of strongly interacting matter was restarted at the beginning of 2000 by the NA49 Collaboration [66]. Fluctuations were analysed in a large number of previously recorded data sets (see Fig. 9 (right)). A tantalizing increase of multiplicity and transverse momentum fluctuations was found in collisions of medium size nuclei at 158A GeV/c. This motivated the ongoing measurements of NA61/SHINE [67], the successor of the NA49 experiment. For the first time, a systematic two-dimensional scan in system size and collision energy is being performed (see Fig. 9 (left)). A search for the critical point is also in progress at RHIC by the STAR Collaboration [3]. Relevant results will be mentioned at the appropriate places. The results from the SPS obtained by NA49 and NA61/SHINE are reviewed below.

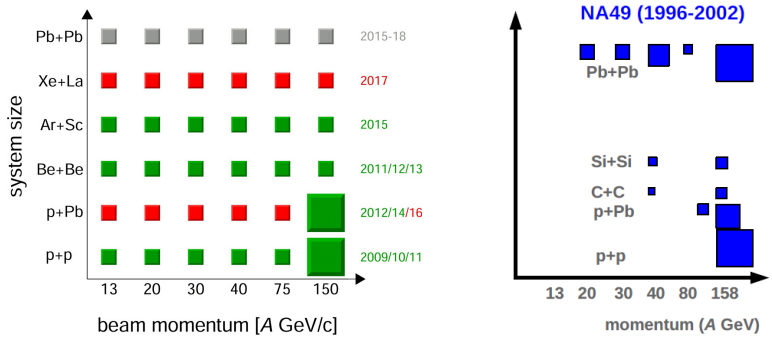

Fig. 9. (Colour on-line) Reactions and energies of the ongoing scan of the phase diagram by NA61 (left) (filled dark grey/green squares denote completion of data taking) and systems previously studied by NA49 (right).

When comparing results from the SPS to those from the RHIC-BES program, one should keep in mind that the event selection and acceptance of the experiments are significantly different. NA49 [68] and NA61/SHINE [69] are fixed-target spectrometers and cover mainly the forward region in the center-

of-mass system, particularly when particle identification is required (see Fig. 10). An advantage of the fixed-target geometry is that it allows to characterise the centrality of the collisions by measuring the energy of the spectators from the beam nucleus independently from the measurements performed on the produced particles. On the other hand, STAR at RHIC is a collider experiment with practically energy-independent rapidity acceptance $|y| \lesssim 0.7$, but without the low transverse momentum region (see curves in Fig. 10). The track density in the detector increases only moderately with collision energy. However, the projectile spectator regions are not accessible to measurement and the collision centrality selection has to be based on the multiplicity of produced particles.

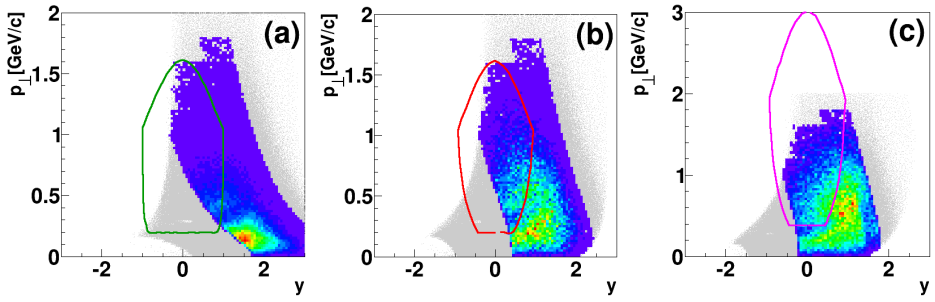

Fig. 10. (Colour on-line) Acceptance of the NA49 and NA61/SHINE experiments for pions (a), kaons (b) and protons (c) at the SPS at 30A GeV (geometrical acceptance in grey, acceptance for identification in colour), as well as that of the STAR detector at RHIC (lines) at the equivalent energy $\sqrt{s_{NN}} = 7.7$ GeV.

3.2.1. Scaled factorial moments

The NA49 experiment at the CERN SPS searched for an intermittency signal in the production of proton [70] and low-mass $\pi^+\pi^-$ pairs [71] in the most central collisions (12%, 12%, 10%) of "C", "Si" and Pb nuclei on C (2.4% interaction length), Si (4.4%) and Pb (1%) targets, respectively, at beam energy of 158A GeV ($\sqrt{s_{NN}} = 17.3$ GeV). The analysis looked in transverse momentum space for a power law behaviour of the second scaled factorial moments (SSFMs, $F_2(M)$) defined in Eq. (1) with $r = 2$.

3.2.2. Intermittency in proton production at mid-rapidity

Protons were identified with a purity of above 80% based on the ionization energy loss of the tracks in the TPC detectors. Poorly measured and fake tracks were carefully removed by suitable selection criteria since they can produce a spurious intermittency signal. Since critical fluctuations

originating from the CP are predicted to be strongest in a region around mid-rapidity in the c.m.s. system, protons were selected in the rapidity range $-0.75 < y < 0.75$.

The strong background from mis-identified and non-critical protons was estimated and subtracted using mixed events, which by construction do not contain critical fluctuations. The resulting SSFMs are plotted in Fig. 11. Evidently, the mixed event background is consistent with the data for "C"+C and Pb+Pb collisions. On the other hand, in "Si"+Si reactions, the values of $F_2(M)$ increase with M^2, while those of the mixed events remain nearly constant.

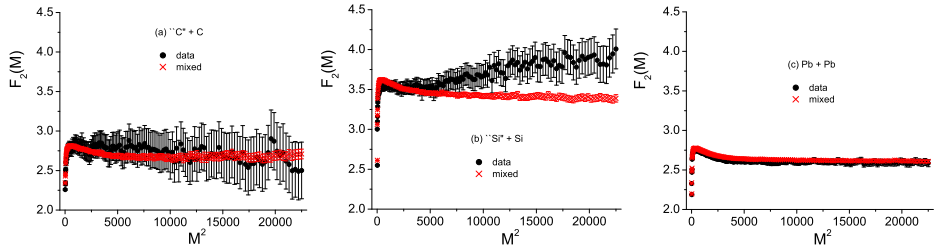

Fig. 11. Second scaled factorial moments $F_2(M)$ of the proton number in transverse momentum space at mid-rapidity ($-0.75 < y < 0.75$) for the most central collisions of (a) "C"+C (12%), (b) "Si"+Si (12%), and (c) Pb+Pb (10%) at $\sqrt{s_{NN}} = 17.3$ GeV. The circles (crosses) represent $F_2(M)$ of the data (mixed events) respectively.

Figure 12 shows the background subtracted SSFMs $F_2^{(e)}(M)$

$$\Delta F_2^{(e)}(M) = F_2^{(d)}(M) - F_2^{(m)}(M)\,, \tag{17}$$

where $F_2^{(d)}(M)$ and $F_2^{(m)}(M)$ correspond to the data and mixed-event background, respectively. While the results for "C"+C and Pb+Pb collisions

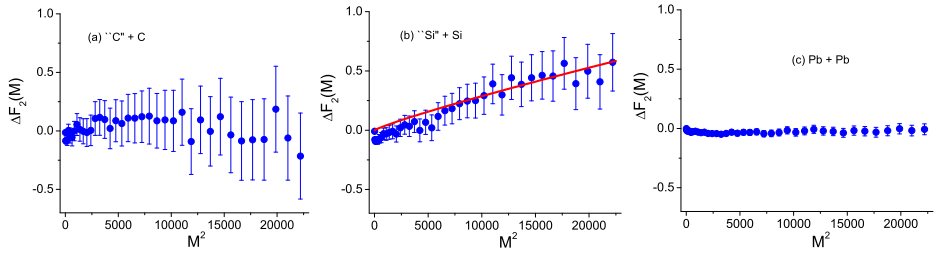

Fig. 12. The combinatorial background subtracted moments $\Delta F_2^{(e)}(M)$ corresponding to the moments of Fig. 11 in bins of transverse momentum for the most central collisions of (a) "C"+C (centrality 12%), (b) "Si"+Si (centrality 12%) and (c) Pb+Pb (centrality 10%) at $\sqrt{s_{NN}} = 17.3$ GeV. The line in the middle plot shows the result of a power-law fit for $M^2 > 6000$ with exponent 0.96.

scatter around zero, the values for "Si"+Si reactions rise with M^2. A power-law fit in the region of $M^2 > 6000$ gave the result $\phi_2 = 0.96^{+0.38}_{-0.25}(\text{stat.}) \pm 0.16(\text{syst.})$ with $\chi^2/\text{d.o.f.} \approx 0.09$–$0.51$. The re-sampling method [72] was used to calculate the errors in order to take account of the strong correlation between successive (in M) values of the SSFMs. Thus, no intermittency signal is present for proton production in "C"+C and Pb+Pb collisions whereas power-law fluctuations are observed in "Si"+Si reactions with an exponent consistent with the CP prediction.

3.2.3. Intermittency in low-mass $\pi^+\pi^-$ pair production

Results of a search for critical fluctuations in the chiral condensate via a similar intermittency study of low-mass $\pi^+\pi^-$ pairs was published by the NA49 Collaboration in Ref. [71]. The chiral condensate is believed to decay into $\pi^+\pi^-$ pairs near the mass threshold when deconfined matter hadronises. As in the case for protons, these fluctuations may be detectable by studying SSFMs of the $\pi^+\pi^-$ pair number, provided the combinatorial background can be sufficiently reduced.

Pions were required to have laboratory momenta exceeding 3 GeV/c and identification was based on the ionization energy loss of the tracks in the TPC detectors. For further analysis, low-mass $\pi^+\pi^-$ pairs satisfying

$$2m_\pi + \epsilon_1 \leq m_{\pi^+\pi^-} \leq 2m_\pi + \epsilon_2 \tag{18}$$

were considered, where $m_{\pi^+\pi^-}$ is the pair invariant mass, $\epsilon_1 = 5$ MeV was chosen to remove the enhancement of pairs from Coulomb attraction and $\epsilon_2 = 34, 24, 1$ MeV for "C"+C, "Si"+Si, and Pb+Pb respectively was optimised to reduce the combinatorial background. Finally, the remaining background was estimated by pairs from mixed events which were made to satisfy the same criteria.

The SSFMs of the $\pi^+\pi^-$ pair multiplicity distribution *versus* the number of subdivisions M^2 of the transverse momentum phase space are shown in Fig. 13 for pairs from data and from mixed events. The rapidity region covered by the selected pairs essentially extends forward of $y \gtrsim 0.5$. One observes that only for "Si"+Si, the SSFMs rise faster for the data than for the mixed events. The combinatorial background subtracted moments $\Delta F_2(M)$ are plotted *versus* M^2 in Fig. 14. At larger values of M^2, the results are consistent with being constant for "C"+C and Pb+Pb, whereas one finds an increase for the "Si"+Si system. Here, a power law function provides a good fit ($\chi^2/\text{d.o.f.} \approx 0.3$) with an exponent $\Phi_2 = 0.33 \pm 0.04$ where the error was estimated by exploiting the subsample method. The extracted exponent indicates a significant intermittency effect, but is smaller than the expectation for the CP of $\Phi_2 = 0.67$. This might well be a consequence of the difficulty of isolating the $\pi^+\pi^-$ pairs from the σ decays.

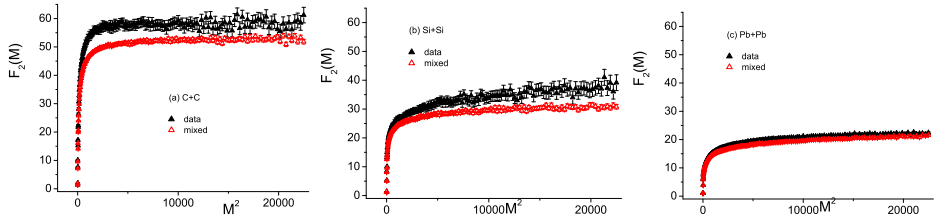

Fig. 13. The second factorial moment $F_2(M)$ in transverse momentum space for: (a) C+C (window of analysis [285, 314] MeV), (b) Si+Si (window of analysis [300.9, 304] MeV) and (c) Pb+Pb (window of analysis [285, 286] MeV) systems. The full triangles represent the moments of NA49 data, while the open triangles, the moments for the corresponding mixed events.

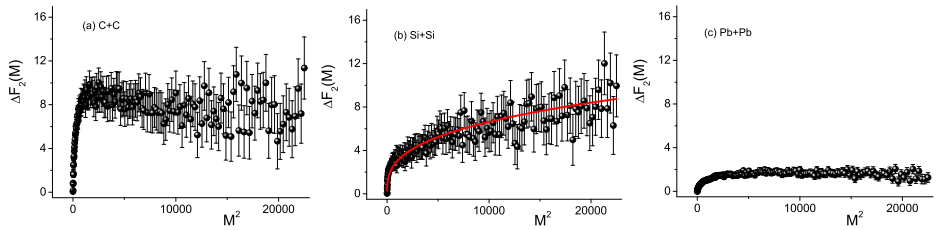

Fig. 14. The combinatorial background subtracted moments ΔF_2 in transverse momentum space for: (a) C+C, (b) Si+Si and (c) Pb+Pb systems. The line in (b) shows the result of a power-law fit for $M^2 > 2000$ with exponent 0.33.

Recently, another analysis method was developed to estimate critical exponents of fluctuations arising from the existence of a CP. This technique studies finite size scaling of the particle source size parameters as obtained from Bose–Einstein interferometry analysis [73]. The results based on RHIC and LHC measurements were interpreted as a possible indication of the CP, however located at a value of μ_B beyond the range accessible in the SPS energy range.

3.2.4. Fluctuations of charged particle multiplicity

The signature of the CP is expected to be primarily an increase of multiplicity fluctuations [15] which are usually quantified by the scaled variance $\omega = (\langle N^2 \rangle - \langle N \rangle^2)/\langle N \rangle$ of the distribution of particle multiplicities N produced in the collisions. The measure ω is intensive, *i.e.* it is independent of the system volume in statistical models within the GCE formulation. However, ω is sensitive to the unavoidable volume fluctuations [50]. Therefore, the measurements were restricted to the 1% most central collisions. This selection is based on the energy deposited by beam spectator nucleons in the

forward calorimeter. Although this tightly constrains the number of projectile participants, small fluctuations of the number of the target participants remain (see model calculations of Ref. [74]).

Results for ω of charged particles in Pb+Pb collisions (NA49 [75]) are shown in Fig. 15 *versus* μ_B[3] and compared to preliminary NA61 results from $p+p$ interactions [76, 77]. Evidently, the energy dependence of ω for the forward hemisphere (which represents almost the full acceptance of NA49 and NA61/SHINE) is smooth without significant maxima. Note that at high SPS energies, ω measured in inelastic $p+p$ interactions is significantly larger than the one for central Pb+Pb collisions. The interpretation of this effect is under discussion [77, 78].

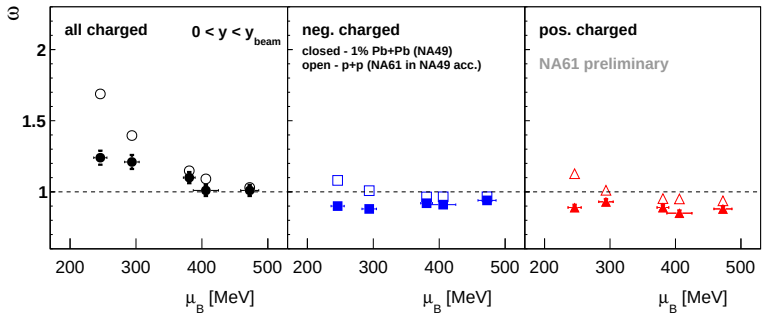

Fig. 15. Scaled variance ω of the multiplicity distribution of charged particles *versus* μ_B for the 1% most central Pb+Pb collisions and inelastic $p+p$ reactions for $0 < y < y_{beam}$ (assuming the pion mass). Full symbols show results of NA49 [75], open symbols preliminary measurements of NA61/SHINE [76, 77].

Figure 16 presents the scaled variance ω of charged particles in the rapidity interval $1.0 < y < y_{beam}$ where the azimuthal acceptance of the detector is high and uniform at all energies. Again, no significant irregularities are observed.

Fluctuations induced by the CP are expected to be stronger at low transverse momenta p_T [79]. Therefore, ω was also calculated for $p_T < 0.3$ GeV/c and < 0.5 GeV/c. The results are plotted in Fig. 17 [75] and turned out to be very similar.

The effects of a hypothetical critical point at $\mu_B = 360$ MeV are illustrated by the curves in Fig. 16 [80]. Assuming $\xi = 3$ fm, the value of ω was estimated to increase by 0.5 (respectively 0.25) for all charged (negatively or positively) charged particles [15, 79] with respect to the value expected for the background fluctuations. The limited acceptance of the detector is

[3] μ_B was obtained from statistical model fits to yields of different particle types at the various collision energies [19]. It is a monotonically decreasing function of collision energy.

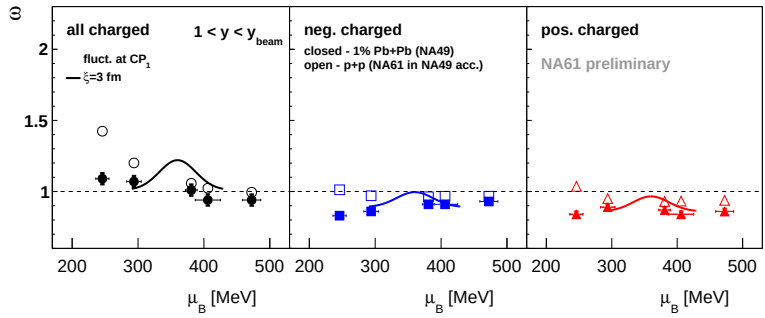

Fig. 16. Scaled variance ω of the multiplicity distribution of charged particles *versus* μ_{B} for the 1% most central Pb+Pb collisions and inelastic $p+p$ reactions for $1.0 < y < y_{\mathrm{beam}}$ (assuming the pion mass). Full symbols show results of NA49 [75], open symbols preliminary measurements of NA61/SHINE [76, 77]. Curves illustrate the effect of a critical point [80].

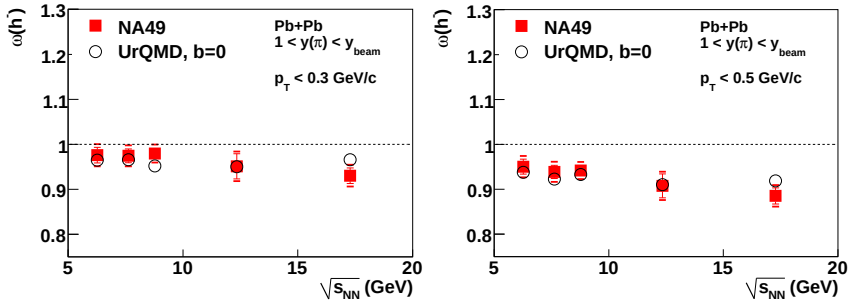

Fig. 17. Scaled variance ω of the multiplicity distribution of negatively charged particles *versus* μ_{B} in the 1% most central Pb+Pb collisions for $1.0 < y < y_{\mathrm{beam}}$ (assuming the pion mass) [75]. Left: $p_{\mathrm{T}} < 0.3$ GeV/c. Right: $p_{\mathrm{T}} < 0.5$ GeV/c. Full symbols show data, open symbols are results from the UrQMD model.

expected to reduce the increase by a factor of the order of 0.6 [75]. Guided by the considerations of Ref. [38] on the region over which the effects of the CP increase the fluctuations, a parameterization by a Gaussian function in μ_{B} was chosen with $\sigma(\mu_{\mathrm{B}}) \approx 30$ MeV. Evidently, the data do not support a maximum as might be expected for a CP (see solid curves in Fig. 16).

NA49 also obtained ω for smaller size nuclei at the top SPS energy of 158A GeV [81]. The results together with those for inelastic $p+p$ collisions from NA49 and NA61/SHINE are plotted in Fig. 18. Interestingly, there may be an indication of a maximum for medium size nuclei.

A new identification procedure (the identity method [82, 83]) was developed which allows to determine the second and third moments of the multiplicity distribution when the particle identification is not unique but

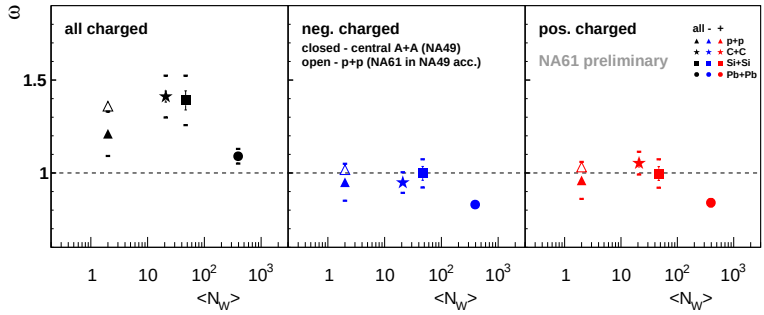

Fig. 18. Scaled variance ω of the multiplicity distribution of charged particles *versus* the number of wounded nucleons N_{W} in inelastic $p+p$ ($1.1 < y < 2.6$) and the 1% most central "C"+C, "Si"+Si and Pb+Pb collisions at 158A GeV ($1.0 < y < y_{\mathrm{beam}}$). Full symbols show results of NA49 [75], open symbols NA61/SHINE [76, 77].

can only be done on a statistical basis. Applying this method, NA49 and NA61/SHINE determined the scaled variance of the multiplicity distribution of identified protons, kaons and pions in inelastic $p+p$ and 3.5% most central Pb+Pb collisions. The results are shown in Fig. 19. As in the case of ω for unidentified charged particles, no indication of the CP is found. It was pointed out that higher moments of the multiplicity distributions are more sensitive to effects of the CP [48]. The STAR Collaboration at RHIC performed such a study for the net-proton multiplicity in central Au+Au collisions at energies in the range of $\sqrt{s_{NN}}$ = 7.7–200 GeV [84], but also found no evidence for the CP.

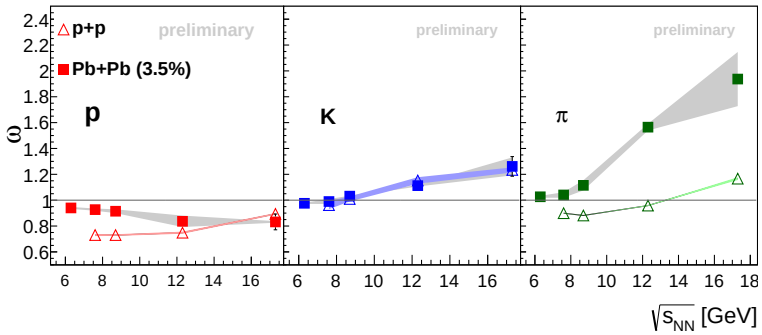

Fig. 19. Scaled variance ω of the multiplicity distribution of protons, kaons, and pions *versus* nucleon–nucleon c.m.s. energy $\sqrt{s_{NN}}$ for the 3.5% most central Pb+Pb collisions (NA49, full symbols) and inelastic $p+p$ reactions (NA61/SHINE, open symbols). Large fluctuations for pions in central Pb+Pb collisions at high energies are likely due to volume fluctuations. Results are preliminary [17].

3.2.5. Fluctuations of the net charge

Fluctuations of the net charge were originally studied in collisions of heavy nuclei in an attempt to find evidence for a deconfined phase. The NA49 Collaboration concluded that the measurements at CERN SPS energies [85] were not sensitive to the initial fluctuations in the QGP since they get masked by the effects of resonance decays. The search for the CP has rekindled interest in this observable because the CP might enhance net-charge fluctuations when the system freezes out in its vicinity.

Fluctuations of the net charge were quantified by the measure Φ proposed in Ref. [52] and defined in Eq. (12). For the case of charge fluctuations, x is taken to be the electric charge q and the measure is called Φ_q.

The distribution of net-charge $Q = \sum_{i=1}^{N} q_i$ in real and mixed events is shown in Fig. 20, where the sum runs over the N particles of the individual events. One observes a clear narrowing effect due to charge conservation, which needs to be corrected. In a scenario in which particles are correlated only by global charge conservation (GCC), the value of Φ_q is given by

$$\Phi_{q,\mathrm{GCC}} = \sqrt{1-P} - 1\,, \tag{19}$$

where

$$P = \frac{\langle N_{\mathrm{ch}} \rangle}{\langle N_{\mathrm{ch}} \rangle_{\mathrm{tot}}} \tag{20}$$

with $\langle N_{\mathrm{ch}} \rangle$ and $\langle N_{\mathrm{ch}} \rangle_{\mathrm{tot}}$ being the mean charged multiplicity in the detector acceptance and in full phase space (excluding spectator nucleons), respectively. In order to remove the sensitivity to GCC, the measure $\Delta\Phi_q$ is defined as the difference

$$\Delta\Phi_q = \Phi_q - \Phi_{q,\mathrm{GCC}}\,. \tag{21}$$

By construction, the value of $\Delta\Phi_q$ is zero if the particles are correlated by global charge conservation only. It is negative in the case of an additional correlation between positively and negatively charged particles, and it is positive if the positive and negative particles are anti-correlated.

Figure 21 [85] demonstrates that the observed net-charge fluctuations are close to the expectation for global charge conservation for all the selected bands of rapidity (the charged particle multiplicity in the band was used as abscissa). The values $\Delta\Phi_q$ stay small at all SPS energies. As shown by the energy dependence of $\Delta\Phi_q$ for two rapidity intervals in Fig. 22, one does not observe a peak structure. The STAR Collaboration at RHIC performed a study of the higher moments of the net-charge distribution in central Au+Au collisions at energies in the range of $\sqrt{s_{NN}} = 7.7$–200 GeV [86] and, so far, also found no evidence for the CP.

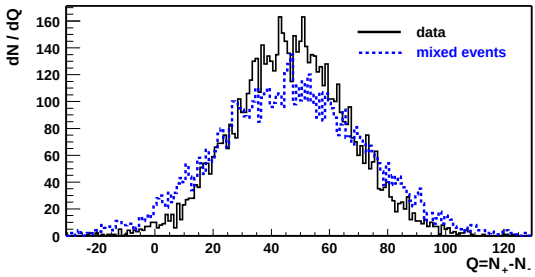

Fig. 20. The distribution of the net-charge for central Pb+Pb collisions at 158A GeV (solid line) and the corresponding distribution obtained for mixed events (dotted line) in the maximum rapidity interval $\Delta y = 3$.

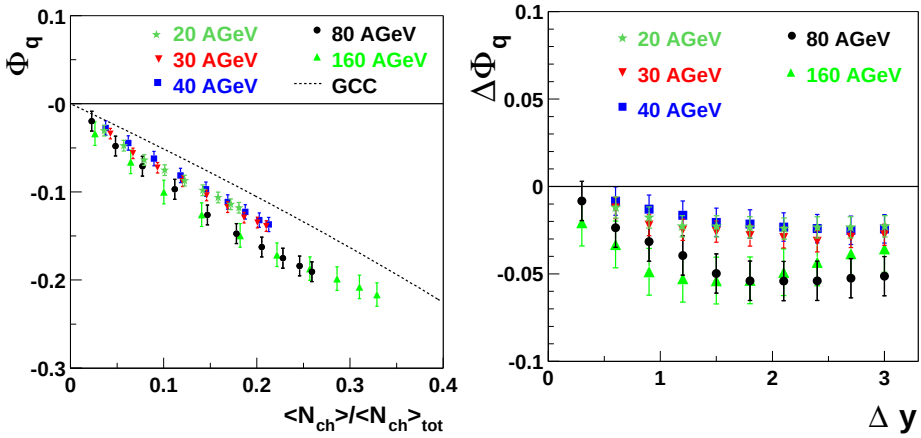

Fig. 21. Left: The dependence of the measure Φ_q on the fraction of accepted particles for central Pb+Pb collisions at 20A–158A GeV. The dashed line shows the dependence expected for the case when the only source of particle correlations is global charge conservation. Right: The dependence of $\Delta\Phi_q$ on the width of the rapidity interval Δy for central Pb+Pb collisions at 20A–158A GeV. Note that experimental points for a given energy are correlated as the data used for a given rapidity interval are included in the broader intervals.

3.2.6. Transverse momentum–multiplicity fluctuations

Enhancement is also expected for transverse momentum–multiplicity fluctuations when the freeze-out occurs close to the CP [15]. For the case of transverse momentum–multiplicity fluctuations, the fluctuation measures Δ and Σ with the IPM normalisation (see Sec. 2.4) read

$$\Delta[P_{\mathrm{T}}, N] = \frac{1}{\langle N\rangle\omega[p_{\mathrm{T}}]}[\langle N\rangle\omega[P_{\mathrm{T}}] - \langle P_{\mathrm{T}}\rangle\omega[N]] \tag{22}$$

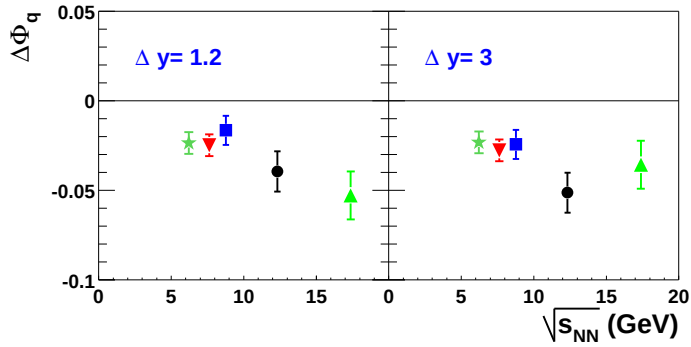

Fig. 22. The energy dependence of $\Delta\Phi_q$ measured in central Pb+Pb collisions at 20A, 30A, 40A, 80A and 158A GeV for a narrow rapidity interval $\Delta y = 1.2$ (left) and a broad rapidity interval $\Delta y = 3$ (right).

and

$$\Sigma[P_{\mathrm{T}}, N] = \frac{1}{\langle N\rangle\omega[p_{\mathrm{T}}]}[\langle N\rangle\omega[P_{\mathrm{T}}] + \langle P_{\mathrm{T}}\rangle\omega[N] - 2(\langle P_{\mathrm{T}}N\rangle - \langle P_{\mathrm{T}}\rangle\langle N\rangle)]\,, \quad (23)$$

where

$$\omega[P_{\mathrm{T}}] = \frac{\langle P_{\mathrm{T}}^2\rangle - \langle P_{\mathrm{T}}\rangle^2}{\langle P_{\mathrm{T}}\rangle} \quad (24)$$

and

$$\omega[N] = \frac{\langle N^2\rangle - \langle N\rangle^2}{\langle N\rangle} \quad (25)$$

are the scaled variances of the two fluctuating extensive event quantities P_{T}, the sum of the absolute values of transverse momenta p_{T}, and N, the number of particles, respectively. The quantity $\omega[p_{\mathrm{T}}]$ is the scaled variance of the inclusive p_{T} distribution (summation runs over all particles and all events)

$$\omega[p_{\mathrm{T}}] = \frac{\overline{p_{\mathrm{T}}^2} - \overline{p_{\mathrm{T}}}^2}{\overline{p_{\mathrm{T}}}}\,. \quad (26)$$

There is an important difference between $\Delta[P_{\mathrm{T}}, N]$ and $\Sigma[P_{\mathrm{T}}, N]$. Only the first two moments: $\langle P_{\mathrm{T}}\rangle$, $\langle N\rangle$, and $\langle P_{\mathrm{T}}^2\rangle$, $\langle N^2\rangle$ are required to calculate $\Delta[P_{\mathrm{T}}, N]$, whereas $\Sigma[P_{\mathrm{T}}, N]$ includes the correlation term $\langle P_{\mathrm{T}} \cdot N\rangle$. Thus, the measures $\Delta[P_{\mathrm{T}}, N]$ and $\Sigma[P_{\mathrm{T}}, N]$ can be sensitive to specific fluctuations in different ways. Both measures are dimensionless and have a common scale required for a quantitative comparison of fluctuations of different, in general dimensional, extensive quantities. The values of Δ and Σ are equal to zero in the absence of event-by-event fluctuations and equal to one for fluctuations given by the model of independent particle production.

The measure $\Phi_{p_{\mathrm{T}}}$ is related to the quantity Σ (see Eq. (14))

$$\Phi_{p_{\mathrm{T}}} = \sqrt{\overline{p_{\mathrm{T}}}\omega[p_{\mathrm{T}}]}\left[\sqrt{\Sigma[P_{\mathrm{T}}, N]} - 1\right] . \tag{27}$$

Results on the dependence of $\Phi_{p_{\mathrm{T}}}$ on μ_{B} ($\sqrt{s_{NN}}$) in central Pb+Pb (NA49 [87]) and inelastic $p+p$ collisions (NA61/SHINE preliminary [76, 77]) are plotted in Fig. 23 (top). The measurements are compared to expectations for the CP (solid curves in Fig. 23 (top) [80]) which were obtained in a similar manner like the predictions for ω under the assumption that the increase of $\Phi_{p_{\mathrm{T}}}$ at the CP amounts to 10 MeV/c for a correlation length of $\xi = 3$ fm. However, more recent theoretical estimates [49] found much less sensitivity of p_{T} fluctuations to the CP.

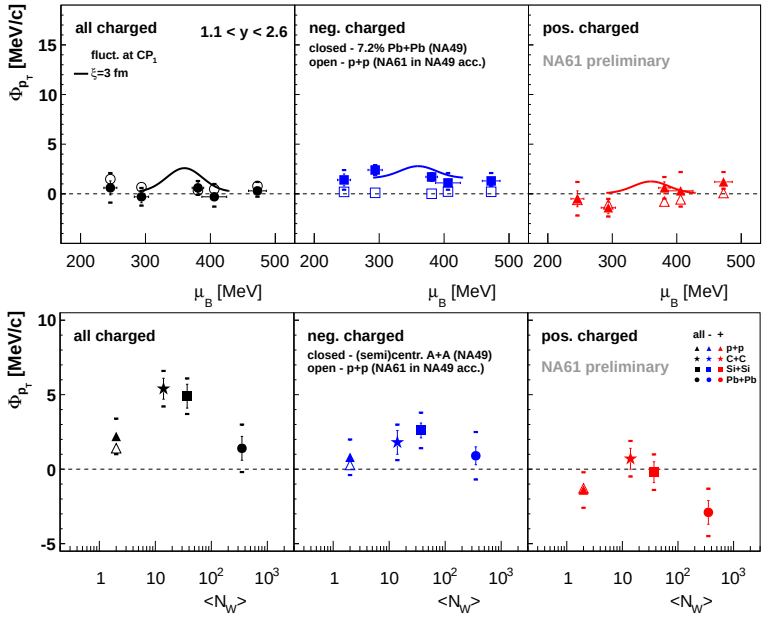

Fig. 23. Measure $\Phi_{p_{\mathrm{T}}}$ of transverse momentum–multiplicity fluctuations of charged particles. Top: *versus* μ_{B} for the 7.2% most central Pb+Pb collisions (full symbols, NA49 [87]) and inelastic $p + p$ reactions (open symbols, NA61/SHINE [76, 77]). Bottom: *versus* the number of wounded nucleons N_{W} in central C+C, Si+Si and Pb+Pb collisions at 158A GeV (NA49 [88]) and inelastic $p + p$ interactions (NA61/SHINE preliminary [76, 77]). Results are for c.m.s. rapidity $1.1 < y < 2.6$ assuming the pion mass. Curves illustrate the effect of the critical point [80].

Some results on Φ_{p_T} for charged particles from central Au+Pb collisions were published by the CERES experiment [90] at the SPS for beam energies of 40A, 80A and 158A GeV. The results in the pseudo-rapidity acceptance of the experiment ($2.2 < \eta < 2.7$) are 1.1 ± 0.4, 2.3 ± 0.8 and 3.3 ± 0.7 MeV, respectively for the 5% most central collisions with systematic uncertainties of the order of 1.5 MeV. In order to account for a possible change of mean p_T at different beam energies, CERES defined a dimensionless measure, the "normalised dynamical fluctuation" Σ_{p_T}

$$\Sigma_{p_\mathrm{T}} \equiv \mathrm{sgn}\left(\sigma^2_{p_\mathrm{T},\mathrm{dyn}}\right) \cdot \frac{\sqrt{\left|\sigma^2_{p_\mathrm{T},\mathrm{dyn}}\right|}}{\overline{p_\mathrm{T}}} \,. \tag{28}$$

Figure 24 shows that there is no significant energy dependence of this measure.

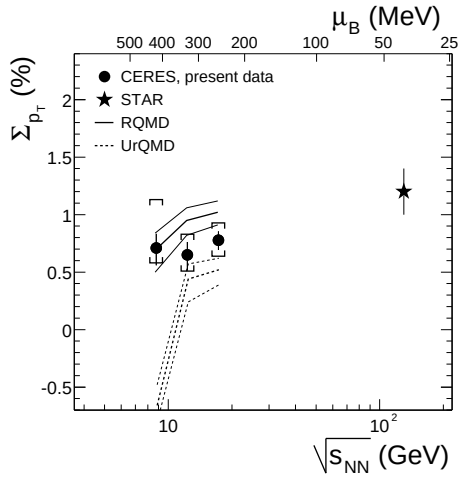

Fig. 24. The fluctuation measure Σ_{p_T} as a function of $\sqrt{s_{NN}}$ and of μ_B [90]. The full circles show CERES results (after short-range correlation (SRC) removal) in central Au+Pb collisions at 40, 80, and 158A GeV/c in the pseudo-rapidity range $2.2 < \eta < 2.7$. The brackets indicate the systematic errors. Also shown is the STAR result [89] at $\sqrt{s_{NN}} = 130$ GeV which is not corrected for SRC. Results and statistical errors from RQMD and UrQMD calculations (with re-scattering) are indicated as solid and dashed lines, respectively.

Measurements by NA49 for different size nuclei at the top SPS energy of 158A GeV are shown in Fig. 23 (bottom). As found for multiplicity fluctuations, there may also be a maximum of transverse momentum fluctuations in medium-size nuclei.

The corresponding results on $\Sigma[P_{\mathrm{T}}, N]$ [17] are presented in Fig. 25. As expected from the close relation with $\Phi_{p_{\mathrm{T}}}$, they indeed show behaviour consistent with that of $\Phi_{p_{\mathrm{T}}}$. Results on $\Delta[P_{\mathrm{T}}, N]$ [17] are shown in Fig. 26. At present, there are no predictions for the effect of the CP in these observables.

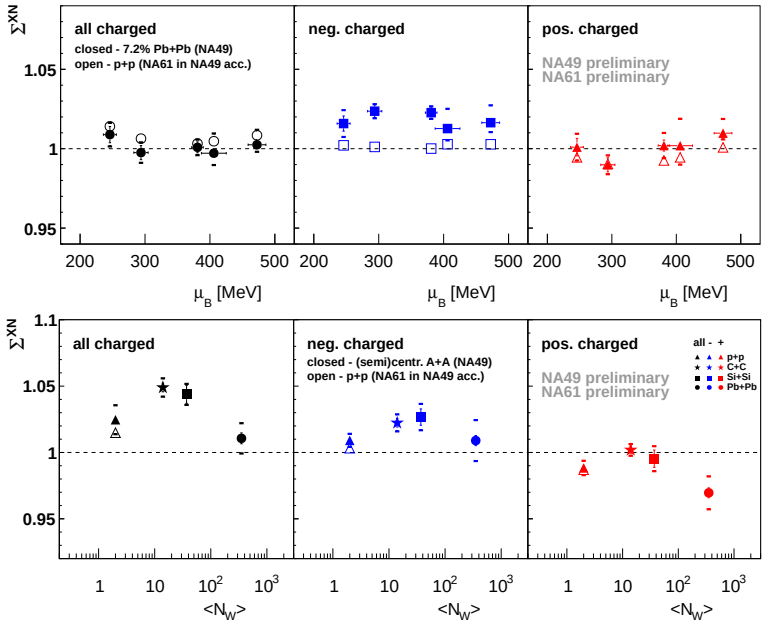

Fig. 25. Measure $\Sigma[P_{\mathrm{T}}, N]$ $(= \Sigma^{P_{\mathrm{T}},N})$ of transverse momentum–multiplicity fluctuations of charged particles. Top: *versus* μ_{B} for the 7.2% most central Pb+Pb collisions (full symbols) and inelastic $p+p$ reactions (open symbols). Bottom: *versus* the number of wounded nucleons N_{W} in inelastic $p+p$ and central "C"+C, "Si"+Si and Pb+Pb collisions at 158A GeV. Results are for c.m.s. rapidity $1.1 < y < 2.6$ assuming the pion mass (NA49 and NA61/SHINE [76, 77]).

Finally, NA61/SHINE results [76, 77] from the two-dimensional scan in system size and collision energy are presented in Fig. 27. The data come from inelastic $p+p$ interactions and centrality selected Be+Be collisions. No indication of the "critical hill" is observed.

Data on Ar+Sc collisions at 13A, 19A, 30A, 40A, 75A and 150A GeV/c are already recorded by NA61/SHINE. They may lead to the discovery of the critical point of strongly interacting matter as possibly suggested by the first indications seen by the NA49 experiment and discussed in this review.

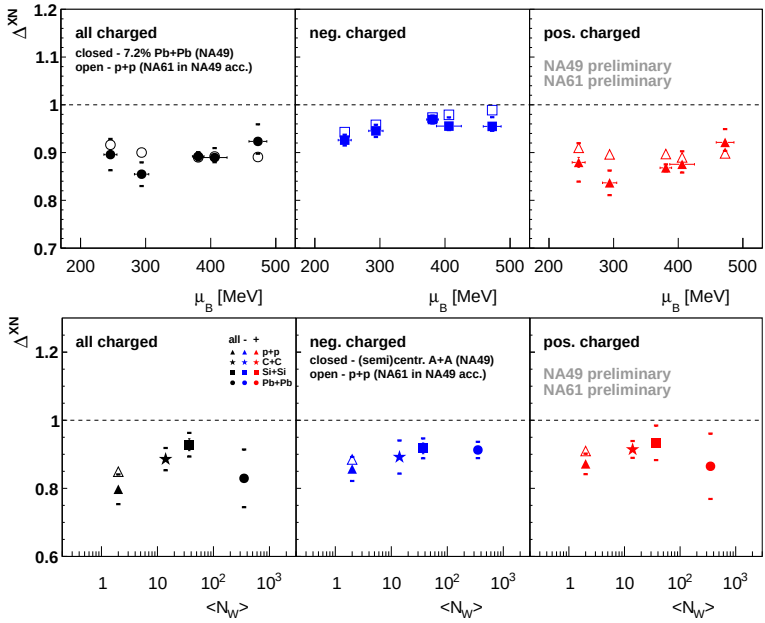

Fig. 26. Measure $\Delta[P_{\mathrm{T}}, N]$ ($= \Delta^{P_{\mathrm{T}},N}$) of transverse momentum–multiplicity fluctuations of charged particles. Top: *versus* μ_{B} for the 7.2% most central Pb+Pb collisions (full symbols) and inelastic $p+p$ reactions (open symbols). Bottom: *versus* the number of wounded nucleons N_{W} in inelastic $p+p$ and central C+C, Si+Si and Pb+Pb collisions at 158A GeV. Results are for c.m.s. rapidity $1.1 < y < 2.6$ assuming the pion mass (NA49 and NA61/SHINE [76, 77]).

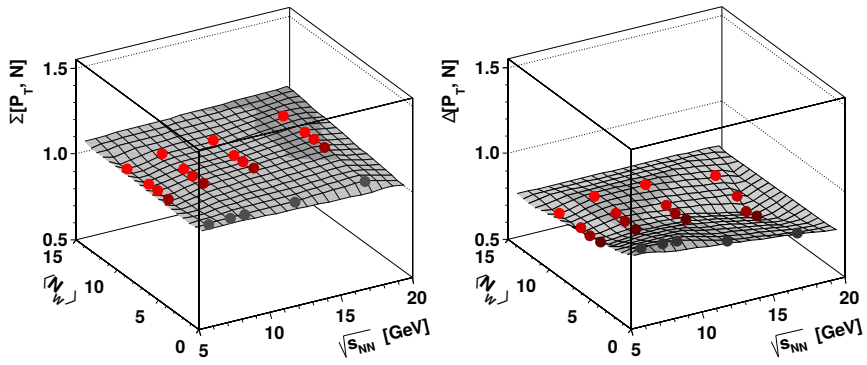

Fig. 27. Preliminary NA61/SHINE results on $\Sigma[P_{\mathrm{T}}, N]$ and $\Delta[P_{\mathrm{T}}, N]$ for Be+Be collisions of several collision centralities and energies compared with the corresponding results from the energy scan with inelastic $p+p$ interactions [76, 77].

4. Conclusions and outlook

The continuing search in nucleus–nucleus reactions for the maximum of fluctuations predicted for the critical point of strongly interacting matter has not yet turned up firm evidence in collisions of heavy nuclei either at the CERN SPS (central Pb+Pb collisions) or in the RHIC BES program (Au+Au collisions).

It is intriguing that both the fluctuations of quantities integrated over the full experimental acceptance (event multiplicity and transverse momentum) as well as the bin size dependence of the second factorial moment of pion and proton multiplicities in medium-sized Si+Si collisions at 158A GeV/c possibly suggest critical behaviour of the created matter.

These results provide strong motivation for the ongoing systematic scan of the phase diagram by the NA61/SHINE experiment at the SPS (see Fig. 9) and the continuing search at the Brookhaven Relativistic Hadron Collider.

We are grateful to Andrzej Bialas, Tobiasz Czopowicz, Katarzyna Grebieszkow and Mark Gorenstein for help and critical comments. We would like to thank Helmut Satz for the motivation to write this review. This work was supported by the National Science Centre of Poland (grant UMO-2012/04/M/ST2/00816), the German Research Foundation (GA 1480/2-2).

REFERENCES

[1] D.D. Ivanenko, D.F. Kurdgelaidze, *Astrophys.* **1**, 251 (1965) [*Astrofiz.* **1**, 479 (1965)]; N. Itoh, *Prog. Theor. Phys.* **44**, 291 (1970); J.C. Collins, M.J. Perry, *Phys. Rev. Lett.* **34**, 1353 (1975); E.V. Shuryak, *Phys. Rep.* **61**, 71 (1980).

[2] See recent results from the LHC presented at QM2014, Darmstadt, Germany, *Nucl. Phys. A*, **931** (2014).

[3] J. Adams *et al.* [STAR Collaboration], *Nucl. Phys. A* **757**, 102 (2005) [arXiv:nucl-ex/0501009].

[4] C. Alt *et al.* [NA49 Collaboration], *Phys. Rev. C* **77**, 024903 (2008); S. Afanasiev *et al.* [NA49 Collaboration], *Phys. Rev. C* **66**, 054902 (2002).

[5] M. Gazdzicki, M. Gorenstein, P. Seyboth, *Acta Phys. Pol. B* **42**, 307 (2011) [arXiv:1006.1765 [hep-ph]].

[6] M. Gazdzicki, M.I. Gorenstein, P. Seyboth, *Int. J. Mod. Phys. E* **23**, 1430008 (2014) [arXiv:1404.3567 [nucl-ex]].

[7] M. Asakawa, K. Yazaki, *Nucl. Phys. A* **504**, 668 (1989).

[8] A. Barducci *et al.*, *Phys. Lett. B* **231**, 463 (1989).

[9] J. Wosiek, *Acta Phys. Pol. B* **19**, 863 (1988).

[10] A. Bialas, R.B. Peschanski, *Nucl. Phys. B* **273**, 703 (1986).

[11] H. Satz, *Nucl. Phys. B* **326**, 613 (1989).

[12] N.G. Antoniou *et al.*, *Phys. Lett. B* **245**, 619 (1990).

[13] A. Bialas, R.C. Hwa, *Phys. Lett. B* **253**, 436 (1991).

[14] M.A. Stephanov, K. Rajagopal, E.V. Shuryak, *Phys. Rev. Lett.* **81**, 4816 (1998) [arXiv:hep-ph/9806219].

[15] M.A. Stephanov, K. Rajagopal, E.V. Shuryak, *Phys. Rev. D* **60**, 114028 (1999) [arXiv:hep-ph/9903292].

[16] R. Holynski *et al.*, *Phys. Rev. Lett.* **62**, 733 (1989).

[17] T. Anticic *et al.* [NA49 Collaboration], *Phys. Rev. C* **92**, 044905 (2015) [arXiv:1509.04633 [nucl-ex]].

[18] See: http://indico.cern.ch/category/6044/

[19] F. Becattini, J. Manninen, M. Gazdzicki, *Phys. Rev. C* **73**, 044905 (2006) [arXiv:hep-ph/0511092].

[20] J. Cleymans, *EPJ Web Conf.* **95**, 03004 (2015) [arXiv:1412.7045 [hep-ph]].

[21] J. Cleymans, K. Redlich, *Nucl. Phys. A* **661**, 379 (1999) [arXiv:nucl-th/9906065].

[22] P. Braun-Munzinger, K. Redlich, J. Stachel, in: R.C. Hwa, X.-N. Wang (Eds.), *Quark–Gluon Plasma 3*, World Scientific Publishing, 2004, pp. 491–599 [arXiv:nucl-th/0304013].

[23] F. Becattini, U.W. Heinz, *Phys. Rev. C* **76**, 269 (1997) [*Erratum ibid.* **76**, 578 (1997)] [arXiv:hep-ph/9702274]; F. Becattini, M. Gazdzicki, J. Sollfrank, *Eur. Phys. J. C* **5**, 143 (1998) [arXiv:hep-ph/9710529].

[24] C. Alt *et al.* [NA49 Collaboration], *Phys. Rev. C* **77**, 024903 (2008) [arXiv:0710.0118 [nucl-ex]].

[25] M. Gazdzicki, *Acta Phys. Pol. B* **45**, 2319 (2014).

[26] M. Gazdzicki *et al.* [NA49-future Collaboration], *PoS* **CPOD2006**, 016 (2006) [arXiv:nucl-ex/0612007].

[27] E.S. Bowman, J.I. Kapusta, *Phys. Rev. C* **79**, 015202 (2009) [arXiv:0810.0042 [nucl-th]].

[28] M.A. Stephanov, *Prog. Theor. Phys. Suppl.* **153**, 139 (2004) [*Int. J. Mod. Phys. A* **20**, 4387 (2005)] [arXiv:hep-ph/0402115].

[29] M. Stephanov, *PoS* **LAT2006**, 24 (2006).

[30] M.G. Alford, K. Rajagopal, F. Wilczek, *Phys. Lett. B* **422**, 247 (1998) [arXiv:hep-ph/9711395]; L. McLerran, R.D. Pisarski, *Nucl. Phys. A* **796**, 83 (2007) [arXiv:0706.2191 [hep-ph]].

[31] N. Antoniou *et al.* [NA61/SHINE Collaboration], CERN-SPSC-2006-034.

[32] A. Bialas, M. Gazdzicki, *Phys. Lett. B* **252**, 483 (1990).

[33] A. Bialas, J. Seixas, *Phys. Lett. B* **250**, 161 (1990).

[34] W. Ochs, J. Wosiek, *Phys. Lett. B* **214**, 617 (1988).

[35] W. Ochs, *Phys. Lett. B* **247**, 101 (1990).

[36] N.G. Antoniou *et al.*, *Nucl. Phys. A* **693**, 799 (2001) [arXiv:hep-ph/0012164].

[37] N.G. Antoniou, Y.F. Contoyiannis, F.K. Diakonos, G. Mavromanolakis, *Nucl. Phys. A* **761**, 149 (2005) [arXiv:hep-ph/0505185].

[38] Y. Hatta, T. Ikeda, *Phys. Rev. D* **67**, 014028 (2003) [arXiv:hep-ph/0210284].

[39] K. Fukushima, T. Hatsuda, *Rep. Prog. Phys.* **74**, 014001 (2011) [arXiv:1005.4814 [hep-ph]].

[40] N.G. Antoniou, F.K. Diakonos, A.S. Kapoyannis, *Phys. Rev. C* **81**, 011901 (2010) [arXiv:0809.0685 [hep-ph]].

[41] F. Karsch, K. Redlich, *Phys. Lett. B* **695**, 136 (2011) [arXiv:1007.2581 [hep-ph]].

[42] V. Skokov, B. Friman, K. Redlich, *Phys. Rev. C* **83**, 054904 (2011) [arXiv:1008.4570 [hep-ph]].

[43] K. Morita, V. Skokov, B. Friman, K. Redlich, *Eur. Phys. J. C* **74**, 2706 (2014) [arXiv:1211.4703 [hep-ph]].

[44] Y. Hatta, M.A. Stephanov, *Phys. Rev. Lett.* **91**, 102003 (2003) [*Erratum ibid.* **91**, 129901 (2003)] [arXiv:hep-ph/0302002].

[45] N.G. Antoniou, F.K. Diakonos, A.S. Kapoyannis, K.S. Kousouris, *Phys. Rev. Lett.* **97**, 032002 (2006) [arXiv:hep-ph/0602051].

[46] V. Vovchenko, D.V. Anchishkin, M.I. Gorenstein, arXiv:1501.03785 [nucl-th].

[47] V. Vovchenko, D.V. Anchishkin, M.I. Gorenstein, R.V. Poberezhnyuk, arXiv:1506.05763 [nucl-th].

[48] M.A. Stephanov, *Phys. Rev. Lett.* **102**, 032301 (2009) [arXiv:0809.3450 [hep-ph]].

[49] C. Athanasiou, K. Rajagopal, M. Stephanov, *Phys. Rev. D* **82**, 074008 (2010) [arXiv:1006.4636 [hep-ph]].

[50] M.I. Gorenstein, M. Gazdzicki, *Phys. Rev. C* **84**, 014904 (2011) [arXiv:1101.4865 [nucl-th]].

[51] M. Gazdzicki, M.I. Gorenstein, M. Mackowiak-Pawlowska, *Phys. Rev. C* **88**, 024907 (2013) [arXiv:1303.0871 [nucl-th]].

[52] M. Gazdzicki, S. Mrowczynski, *Z. Phys. C* **54**, 127 (1992).

[53] E. Sangaline, arXiv:1505.00261 [nucl-th].

[54] B. Berdnikov, K. Rajagopal, *Phys. Rev. D* **61**, 105017 (2000) [arXiv:hep-ph/9912274].

[55] M.I. Gorenstein, arXiv:1505.04135 [nucl-th].

[56] J. Rafelski, M. Danos, *Phys. Lett. B* **97**, 279 (1980).

[57] K. Redlich, L. Turko, *Z. Phys. C* **5**, 201 (1980).

[58] F. Becattini, L. Ferroni, *Eur. Phys. J. C* **35**, 243 (2004) [arXiv:hep-ph/0307061].

[59] V.V. Begun, M. Gazdzicki, M.I. Gorenstein, O.S. Zozulya, *Phys. Rev. C* **70**, 034901 (2004) [arXiv:nucl-th/0404056].

[60] V.V. Begun, M.I. Gorenstein, A.P. Kostyuk, O.S. Zozulya, *Phys. Rev. C* **71**, 054904 (2005) [arXiv:nucl-th/0410044].

[61] I. Derado, G. Jancso, N. Schmitz, P. Stopa, *Z. Phys. C* **47**, 23 (1990).

[62] I.V. Azhinenko *et al.* [EHS/NA22 Collaboration], *Phys. Lett. B* **235**, 373 (1990).

[63] R. Holynski *et al.*, *Phys. Rev. C* **40**, 2449 (1989).

[64] R. Albrecht *et al.* [WA80 Collaboration], *Phys. Rev. C* **50**, 1048 (1994).

[65] J. Bachler *et al.* [NA35 Collaboration], *Z. Phys. C* **61**, 551 (1994).

[66] See: http://na49info.web.cern.ch/na49info/na49/

[67] See: http://shine.web.cern.ch/

[68] S. Afanasiev *et al.* [NA49 Collaboration], *Nucl. Instrum. Methods A* **430**, 210 (1999).

[69] N. Abgrall *et al.* [NA61 Collaboration], *JINST* **9**, P06005 (2014).

[70] T. Anticic *et al.* [NA49 Collaboration], *Eur. Phys. J. C* **75**, 587 (2015) [arXiv:1208.5292 [nucl-ex]].

[71] T. Anticic *et al.* [NA49 Collaboration], *Phys. Rev. C* **81**, 064907 (2010) [arXiv:0912.4198 [nucl-ex]].

[72] B. Efron, *Ann. Stat.* **7**, 1 (1979); T. Hesterberg *et al.*, *Bootstrap Method and Permutation Tests*, W.H. Freeman & Co., 2003, ISBN-10:0716757265.

[73] R.A. Lacey, *Phys. Rev. Lett.* **114**, 142301 (2015) [arXiv:1411.7931 [nucl-ex]].

[74] V.P. Konchakovski *et al.*, *Phys. Rev. C* **73**, 034902 (2006) [arXiv:nucl-th/0511083].

[75] C. Alt *et al.* [NA49 Collaboration], *Phys. Rev. C* **78**, 034914 (2008) [arXiv:0712.3216 [nucl-ex]].

[76] T. Czopowicz [NA61/SHINE Collaboration], arXiv:1503.01619 [nucl-ex].

[77] A. Aduszkiewicz *et al.* [NA61/SHINE Collaboration], arXiv:1510.00163 [hep-ex].

[78] V.P. Konchakovski, M.I. Gorenstein, E.L. Bratkovskaya, *Phys. Lett. B* **651**, 114 (2007) [arXiv:nucl-th/0703052].

[79] M. Stephanov, private communication.

[80] K. Grebieszkow [NA49 Collaboration], *Nucl. Phys. A* **830**, 547C (2009) [arXiv:0907.4101 [nucl-ex]] and M. Stephanov, private communication.

[81] C. Alt *et al.* [NA49 Collaboration], *Phys. Rev. C* **75**, 064904 (2007) [arXiv:nucl-ex/0612010].

[82] M. Gazdzicki, K. Grebieszkow, M. Mackowiak, S. Mrowczynski, *Phys. Rev. C* **83**, 054907 (2011) [arXiv:1103.2887 [nucl-th]].

[83] M.I. Gorenstein, *Phys. Rev. C* **84**, 024902 (2011) [arXiv:1106.4473 [nucl-th]].

[84] L. Adamczyk *et al.* [STAR Collaboration], *Phys. Rev. Lett.* **112**, 032302 (2014) [arXiv:1309.5681 [nucl-ex]].

[85] C. Alt *et al.* [NA49 Collaboration], *Phys. Rev. C* **70**, 064903 (2004) [arXiv:nucl-ex/0406013].

[86] L. Adamczyk *et al.* [STAR Collaboration], *Phys. Rev. Lett.* **113**, 092301 (2014) [arXiv:1402.1558 [nucl-ex]].

[87] T. Anticic *et al.* [NA49 Collaboration], *Phys. Rev. C* **79**, 044904 (2009) [arXiv:0810.5580 [nucl-ex]].

[88] T. Anticic *et al.* [NA49 Collaboration], *Phys. Rev. C* **70**, 034902 (2004) [arXiv:hep-ex/0311009].

[89] S.A. Voloshin [STAR Collaboration], *AIP Conf. Proc.* **610**, 591 (2002) [arXiv:nucl-ex/0109006].

[90] D. Adamova *et al.* [CERES Collaboration], *Nucl. Phys. A* **727**, 97 (2003) [arXiv:nucl-ex/0305002].